Article

Not peer-reviewed version

Antiproliferative, Pro-apoptotic Activity and Tubulin Dynamics Modulation of 1H-Benzimidazole-2-Yl Hydrazones in Human Breast Cancer Cell Line Mda-Mb-231

Denitsa Yancheva *, Maria Argirova, Irina Georgieva, Vanya Milanova, Maya Guncheva, Nadya Hristova-Avakumova, Miroslav Rangelov, Nadezhda Todorova, Rumiana Tzoneva *

Posted Date: 21 March 2024

doi: 10.20944/preprints202403.1210.v1

Keywords: benzimidazole-2-yl hydrazones; tubulin polymerization; mitotic blockage; cytotoxicity; oxidative stress; MDA-MB-231 cells

Article

Antiproliferative, Pro-Apoptotic Activity and Tubulin Dynamics Modulation of 1*H*-Benzimidazole-2-yl Hydrazones in Human Breast Cancer Cell Line MDA-MB-231

Denitsa Yancheva [1,*], Maria Argirova [1], Irina Georgieva [2], Vanya Milanova [2], Maya Guncheva [1], Nadya Hristova-Avakumova [3], Miroslav Rangelov [1], Nadezhda Todorova [4] and Rumiana Tzoneva [2,*]

[1] Institute of Organic Chemistry with Centre of Phytochemistry, Bulgarian Academy of Sciences, Acad. G. Bonchev Str., build. 9, 1113 Sofia, Bulgaria; e-mail@e-mail.com
[2] Institute of Biophysics and Biomedical Engineering, Bulgarian Academy of Sciences, Acad. G. Bonchev Str., build. 21, 1113 Sofia, Bulgaria; e-mail@e-mail.com
[3] Department of Medical Physics and Biophysics, Faculty of Medicine, Medical University of Sofia, 2 Zdrave Str., 1431 Sofia, Bulgaria; e-mail@e-mail.com
[4] Institute of Biodiversity and Ecosystem Research, Bulgarian Academy of Sciences, 2 Gagarin Str., 1113 Sofia, Bulgaria; e-mail@e-mail.com
* Correspondence: tzoneva@bio21.bas.bg (R. Tz.); denitsa.pantaleeva@orgchm.bas.bg (D. Y.)

Abstract: (1) Background: In this work, a series of benzimidazole derivatives containing colchicine-like and cathechol-like moieties with methyl group substitution in the benzimidazole ring were evaluated for their in vitro antiproliferative, pro-apoptotic and antioxidative activity against highly invasive breast cancer cell line MDA-MB-231 and related impairment of tubulin dynamics; (2) Methods: MTT assay was used to evaluate the antiproliferative activity. In vitro tubulin polymerization assay as well as docking analysis was applied to prove the alterations in tubulin polymerization. Immunofluorescent and DAPI staining reveal the pro-apoptotic potential of benzimidazole derivatives and the effect on tubulin's dynamics in living cells. The antioxidant activity was evaluated by scavenging of H_2O_2 and hypochlorite ion and ortho-phenanthroline tests; (3) Results: The compounds containing colchicine-like moiety displayed significant growth inhibitory effect against cancer cell line as was highlighted the role of methyl functional group on the tubulin aggregation and blockage of mitosis. All compounds showed an ability to scavenge H_2O_2, while the compounds with cathecol-like moiety were more effective against hypochlorite ion and chelation of iron; (4) Conclusions: The benzimidazole derivative containing colchicine-like moiety and methyl group substitution in benzimidazole ring is a potential antiproliferative and microtubule destabilizing agent.

Keywords: benzimidazole-2-yl hydrazones; tubulin polymerization; mitotic blockage; cytotoxicity; oxidative stress; MDA-MB-231 cells

1. Introduction

Microtubules are key components of the cytoskeleton that are composed of α-tubulin and β-tubulin heterodimers, forming a 25 nm in diameter, long, filamentous, tube-shaped supramolecular complex. Since they are intrinsically polarized, they are responsible either for regulation and maintenance of cell polarity [1–3]. During the interphase, they span radially, providing tracks for the fast transport of cargoes by members of two classes of molecular motor proteins – dynein and kinesin [4]. During mitosis, microtubules (MTs) rearrange to form the mitotic spindle, composed of MTs stretching from two opposing spindle poles: the minus ends, anchored to the poles, and the plus ends, extending away from them and binding to chromosomes [5]. This machinery is responsible for

 doi:10.20944/preprints202403.1210.v1

the correct alignment and segregation of the chromosomes. Therefore, in this way, the stages of mitosis that cells go through during normal cell division can be studied closely.

Microtubule-targeting agents (MTAs) are a highly successful class of cancer drugs with therapeutic application in both hematopoietic and solid tumors [6]. They exert their antitumor activity by disrupting the microtubules, which induces cell cycle arrest in the G2-M phase due to suppression of spindle-microtubule dynamics. As a result, chromosome segregation is interrupted which could trigger the slowing or blocking of mitosis at the metaphase–anaphase transition and induction of apoptotic cell death [7]. At higher concentrations, the antimitotic drugs reveal their activity by either of two mechanisms - inhibiting microtubules' polymerization thus leading to destabilization, reducing the polymer mass and blocking cell proliferation at metaphase during mitosis, or by initiating the microtubules polymerization, stabilizing them and increasing the polymer mass [3,8–10]. Based on their mechanism of action, antimitotic agents can be divided into two main groups: microtubule-destabilizing agents (MDA), which inhibit microtubule polymerization at high concentrations and include several compounds such as vinca alkaloids (vinblastine, vincristine, etc.) and colchicine, and microtubule-stabilizing agents (MSA), which stimulate microtubule polymerization such as taxanes (paclitaxel and docetaxel) (Figure 1) [3,11,12].

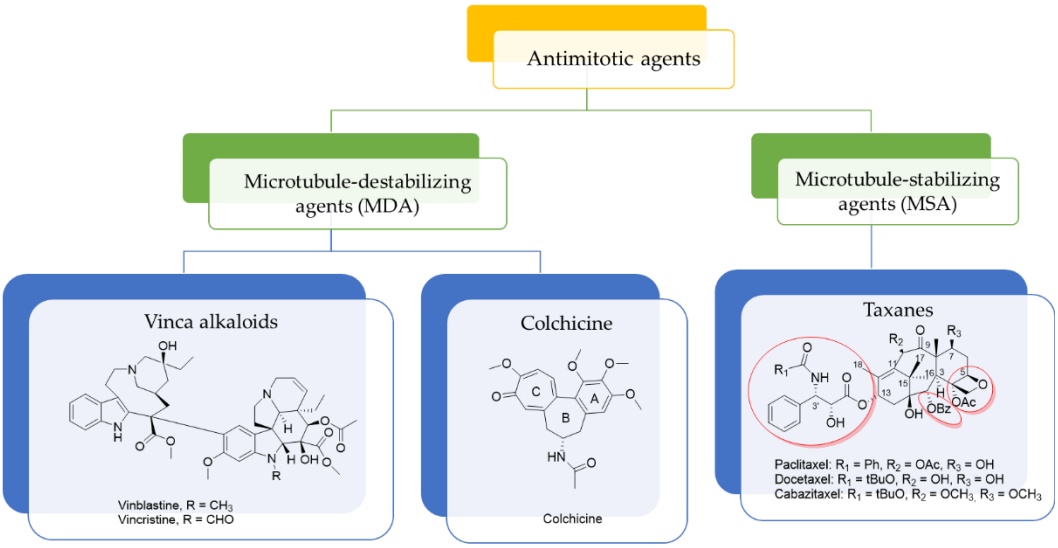

Figure 1. Microtubule-destabilizing and microtubule-stabilizing antimitotic agents targeting different binding sites.

The main groups can be further divided into subgroups based on their targeting of different binding sites on the αβ-tubulin dimer. Currently at least eight binding sites are recognized in the αβ-tubulin dimer, most of them being located on the β-tubulin [13,14]. Research efforts have primarily focused on exploring the binding sites of vinca alkaloids, colchicine, and taxanes. The vinca domain is located at the inter-dimer interface between two longitudinally aligned tubulin dimers. The taxane site is found in a deep hydrophobic pocket at the lateral interface in the microtubule lumen between adjacent protofilaments. Finally, the colchicine site is located at the intra-dimer interface between β-tubulin and α-tubulin. Vinca alkaloids, taxanes and their derivatives have been well studied and some are applied in chemotherapy for different types of cancers [11,12,15]. Among the versatile antimitotic drugs that bind to the colchicine site, the natural products combretastatin A-1 (CA-1) and A-4 (CA-4) and the synthetic compound nocodazole (Figure 2) are the most promising drugs for cancer treatment.

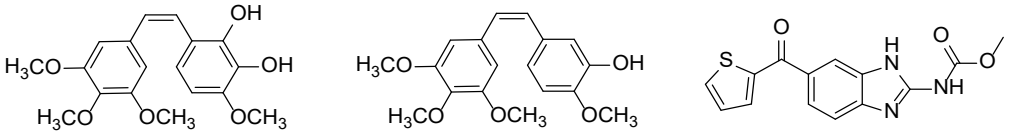

Combretastatin A-1 (CA-1) Combretastatin A-4 (CA-4) Nocodazole

 doi:10.20944/preprints202403.1210.v1

Figure 2. MTAs targeting colchicine binding site on β-tubulin.

CA-1 and CA-4 are stilbene compounds bearing trimethoxypenyl moiety in combination with catechol or vanillin-derived fragment [16]. The water-soluble prodrug of CA-1 – a dipotassium diphosphate derivative (OXi4503) is currently in clinical trials for patients with relapsed or refractory acute myeloid leukemia [17]. Water-soluble phosphate prodrug of CA-4 (fosbretabulin, Zybrestat) and a serine derivative of CA-4 (ombrabulin) are also in clinical trials either alone or in combination with other chemotherapeutics of sradio therapy [18,19]. Nocodazole, a member of the benzimidazole family, attracted the attention due to its potent tubulin inhibition and significant antiproliferative activity and it is widely used in clinical research [12]. Through the years several structural modifications of these drugs have been reported which improved their antitumor activity [15,20,21]. Despite the great number of synthesized compounds targeting the colchicine binding site, no colchicine site inhibitors are still approved for cancer therapy.

The diverse representatives of the benzimidazole family exhibiting potent tubulin polymerization such as denibulin, NSC:761109/1 and 2-aryl-benzimidazoles derivatives of dehydroabietic acid, outlines the benzimidazole nuclei as a useful pharmacophore for the design of novel tubulin polymerization inhibitors [22–26]. Recently we have reported the synthesis of a library 1*H*-benzimidazol-2-yl hydrazones containing hydroxy, methoxy and fluoro groups in the phenyl moiety or 1,3-benzodioxolyl substituent [27,28]. The compounds exhibited excellent in vitro anthelmintic activity against isolated Trichinella spiralis muscle larvae and cytotoxicity against human malignant cell lines MCF-7 and AR-230, and normal fibroblast cell line 3T3 and CCL-1 [27–29]. The compounds also showed radical-scavenging activity against stable free radicals such as DPPH, ABTS and biologically relevant peroxyl radicals, significant protective effect in model systems, containing deoxyribose and lecithin, and metal-chelating activity. The ability to interact with tubulin was studied by molecular docking and in vitro assay of the tubulin polymerization. Most of the compounds elongated the nucleation phase and retarded the tubulin polymerization comparably to nocodazole.

In this study, we extended the evaluation of 1*H*-benzimidazol-2-yl hydrazones by testing their potential antiproliferative and pro-apoptotic activity against highly invasive breast cancer cell line MDA-MB-231 and related impairment of cancer cell's tubulin dynamics of two of the most post promising compounds from the 1*H*-benzimidazol-2-yl hydrazone series (**5a** and **5b**, Scheme 1) and two newly synthesized derivatives with a methyl group in the benzimidazole ring (**5c** and **5d**, Scheme 1). The impact of 1*H*-benzimidazole-2-yl hydrazones on tubulin polymerization was additionally evaluated in vitro us ing purified porcine tubulin to determine the effect of the methyl substitution in the benzimidazole ring and compare it with the microtubule-modulating agents paclitaxel and nocodazole. The interactions of the studied compounds with tubulin were elucidated by molecular docking in the colchicine binding site. The efficacy of the compounds in scavenging hydrogen peroxide and hypochlorite ions, reactive oxygen species (ROS) associated with oxidative stress-related pathways implicated in breast cancer progression, metastasis, and therapy resistance, was assessed in in vitro chemical model systems.

2. Results and Discussion

2.1. Synthesis of Target Compounds

The reaction pathway for synthesis of the target benzimidazolyl hydrazones was carried out as shown in Scheme 1 in accordance with the previously described procedure [27,28]. Briefly, the benzimidazole thiols **2a-b** were obtained by a reaction of carbon disulphide with potassium hydroxide and o-phenylenediamine in an ethanol medium. The benizmidazolyl sulfonic acids **3a-b** was achieved in a 50 % ethanol solution of potassium permanganate under reflux with constant stirring for 1-2 hours, followed by acidification with hydrochloric acid to pH = 1. A reaction of nucleophilic substitution with an excess of hydrazine hydrate afforded 1H-benzimidazole-2-yl hydrazines **4a-b**. In the final step, **4a-b** were reacted with 2,3-hydroxybenzaldehyde or 3,4,5-

 doi:10.20944/preprints202403.1210.v1

trimethoxybenzaldehyde in absolute ethanol and four 1H-benzimidazole-2-yl hydrazones **5a-d** were obtained where the substitution in the benzimidazole ring was varied (a methyl group vs. nonsubstituted ring) along with the phenyl part (catechol-like vs. colchicine-like moiety) (Scheme 1).

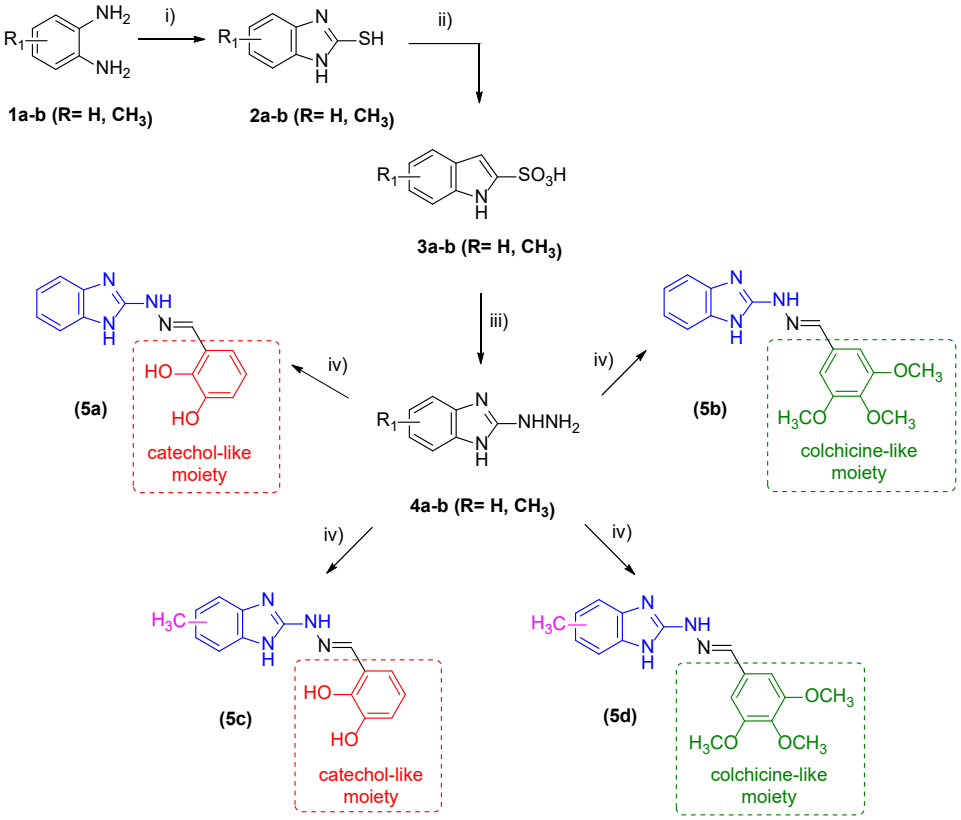

Scheme 1. Reaction pathway for the synthesis of 1*H*-benzimidazole-2-yl hydrazones **5a-d**: i) CS2, KOH, EtOH, refluxing; 50% acetic acid; ii) oxidation in a 50 % ethanol solution of potassium permanganate, 1 h; acidification by hydrochloric acid to pH=1; iii) refluxing in excess of 99% hydrazine hydrate, 3 h; iv) condensation with substituted benzaldehyde in 99 % ethanol, molar ratio 1:1, 3-4 h.

The synthesis of the two 1H-benzimidazole-2-yl hydrazones **5a** and **5b** bearing unsubstituted benzimidazole ring is provided in more detail in our previous publication along with the spectral data confirming their structure [28]. The structures of the newly obtained 1H-benzimidazole-2-yl hydrazones **5c** and **5d** was established by FT-IR, ^{1}H NMR and ^{13}C NMR spectroscopy and the data are provided in the Experimental section. One of the most characteristic bands in the IR spectra is that of the formation of the azomethine bond (C=N) at ca. 1620 cm^{-1}. The N-H group of the benzimidazole ring as well as that of the hydrazine chain, are characterized by the presence of a peak in the region 3370-3250 cm-1. The hydrazone **5c**, containing hydroxyl groups at ortho- and meta positions, showed a band for the C–O stretching vibrations around 1260 cm^{-1}. In the IR spectra of compound **5d** bands for the C–O stretching vibrations of the methoxyl groups were registered within the interval 1270-1050 cm^{-1} with moderate to strong intensity.

In the ^{1}H NMR spectra of the target hydrazones were registered singlets at ca. 8 ppm thus confirming the formation of the azomethine bond. The benzimidazole protons were found as multiplets in the region 6.9–7.3 ppm while those for the phenyl moiety – around 7-7.8 ppm. At 11.35 ppm and 9.35 ppm two broad signals were observed for the protons for the amino and hydroxyl groups. The chemical shifts for the OCH_3 groups varied in the range 3.9-3.7 ppm. The substitution of the benzimidazole ring with a methyl group at 5(6)-position gave rise to a singlet at 2.32-2.40 ppm. In the ^{13}C NMR spectra the signals for the azomethyne C-atoms were found at ca. 141-143 ppm. The C-atoms from the methoxy groups resonate at ca. 56 ppm while those for the methyl group in the benzimidazole cycle were registered at ca. 21 ppm.

 doi:10.20944/preprints202403.1210.v1

2.2. In Vitro Effect on Tubulin Polymerization and Docking Study on the Tubulin-Ligands Interactions

The effect of 1H-benzimidazole-2-yl hydrazones **5a-d** on tubulin polymerization was evaluated in vitro on purified porcine tubulin. The turbidity of the mixtures was monitored at 350 nm for 90 min and compared to nocodazole and paclitaxel as negative and positive controls (Figure 3). The tubulin polymerization assay was carried out at a concentration 10 μM of the reference drugs and compounds **5a-d**.

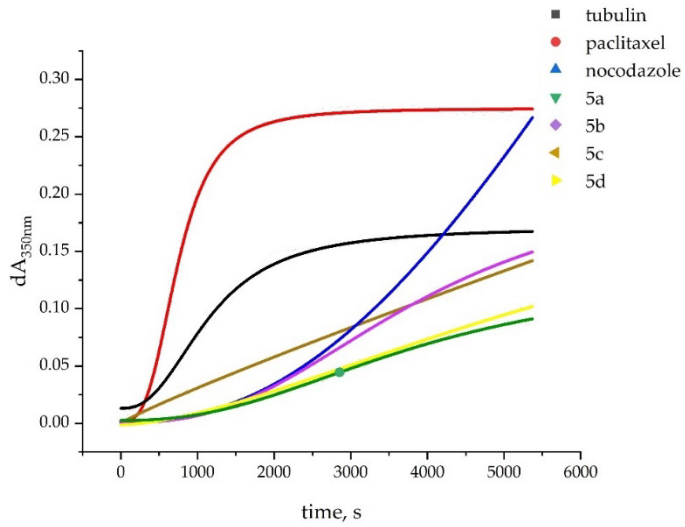

Figure 3. Tubulin (final 54 μM) in presence of PB-GTP buffer, 10 μM paclitaxel, 10 μM nocodazole and 10 μM of the assayed compounds. Reaction was conducted in thermostated spectrophotometric chamber at 37ºC for 90 min. Turbidity was measured at 350 nm every 30 sec.

The in vitro tubulin polymerization assay showed that the spontaneous tubulin polymerization proceeded with an initial rate of 75.3 a.u.sec^{-1}.10^{-6}, while nocodazole delayed the start of the polymerization with 935 sec. and lowered the initial rate to 52 a.u.sec^{-1}.10^{-6} (Table 1). In contrary, paclitaxel accelerated the polymerization to 167 a.u.sec^{-1}.10^{-6}. As reported earlier, the two hydrazones without a substituent in the benzimidazole ring **5a** and **5b** are characterized by 1461 and 988 sec lag time and considerable reduction of the initial rate - 13.4 for **5a** and 20.6 a.u.sec^{-1}.10^{-6} for **5b**, respectively [29]. The introduction of a methyl group in the benzimidazole ring induced slightly different effect on the tubulin polymerization. While **5c** (with catechol-like moiety) showed no lag time and initial rate of polymerization 27 a.u.sec^{-1}.10^{-6}, **5d** (with colchicine-like moiety) delayed the polymerization with 600 sec. followed by polymerization phase with 12.9 a.u.sec^{-1}.10^{-6} rate. Compound **5d**, combining a methyl group in the benzimidazole ring and colchicine-like fragment in the hydrazone chain, exhibited the most significant reduction of the tubulin polymerization rate among the tested compounds.

Table 1. In vitro effect on tubulin polymerization of 1*H*-benzimidazole-2-yl hydrazones **5a-d**, paclitaxel and nocodazole.

Compound	Tubulin polymerization [1]	
	lag time, sec.	initial rate [2]
tubulin (spontaneous polymerization)	no lag phase	75.3
	Unsubstituted benzimidazole ring	
5a [3]	1461	13.4
5b [3]	988	20.6
	5(6)-Methyl benzimidazole ring	
5c	no lag phase	27.0
5d	600	12.9

 doi:10.20944/preprints202403.1210.v1

	Reference compounds	
Paclitaxel [3]	151	167
Nocodazole [3]	935	52

[1] at final conc. of all compounds and standards 10 μM; [2] signal response a.u.sec^{-1}.10^{-6}; [3] data from [29].

Molecular docking study was conducted to provide better insight into the possible binding modes of the 1*H*-benzimidazol-2-yl hydrazones with tubulin using MOE program package [30]. The interactions of the ligands **5a-d** were modeled based on the X-ray structure of the colchicine complex of αβ-tubulin with colchicine and vinblastine, PDB ID: 1Z2B [31]. Previous studies have shown that in the active pocket, the nonsubstituted benzimidazole ring of ligands **5a** and **5b** is oriented towards the hydrophobic amino acid residues of β-tubulin and the phenyl moiety, either catechol-like or colchicine-like, faces the polar amino acid residues of α-tubulin. In the case of methyl-substituted ligands **5c** and **5d** the phenyl rings lie again in a close distance to the GTP and some of the key amino acid residues which are believed to be important for the interactions preventing the "curved-to-straight" conformational change during the tubulin assembly – the polar amino acid residues Ser178 and Thr179 of α-tubulin T5 loop, Gln11 in T1 loop of α-tubulin or Lys254 within the H8 helix of β-tubulin [25,32,33]. The interaction maps of ligands **5c-d** (Figure 4) indicated that the binding of **5c** and **5d** is based mainly on Van der Waals interactions and in the case of **5d** – also some lipophilic interactions between the trimethoxyphenyl ring and Lys254 from the β-tubulin unit, positioned in close proximity to the GTP.

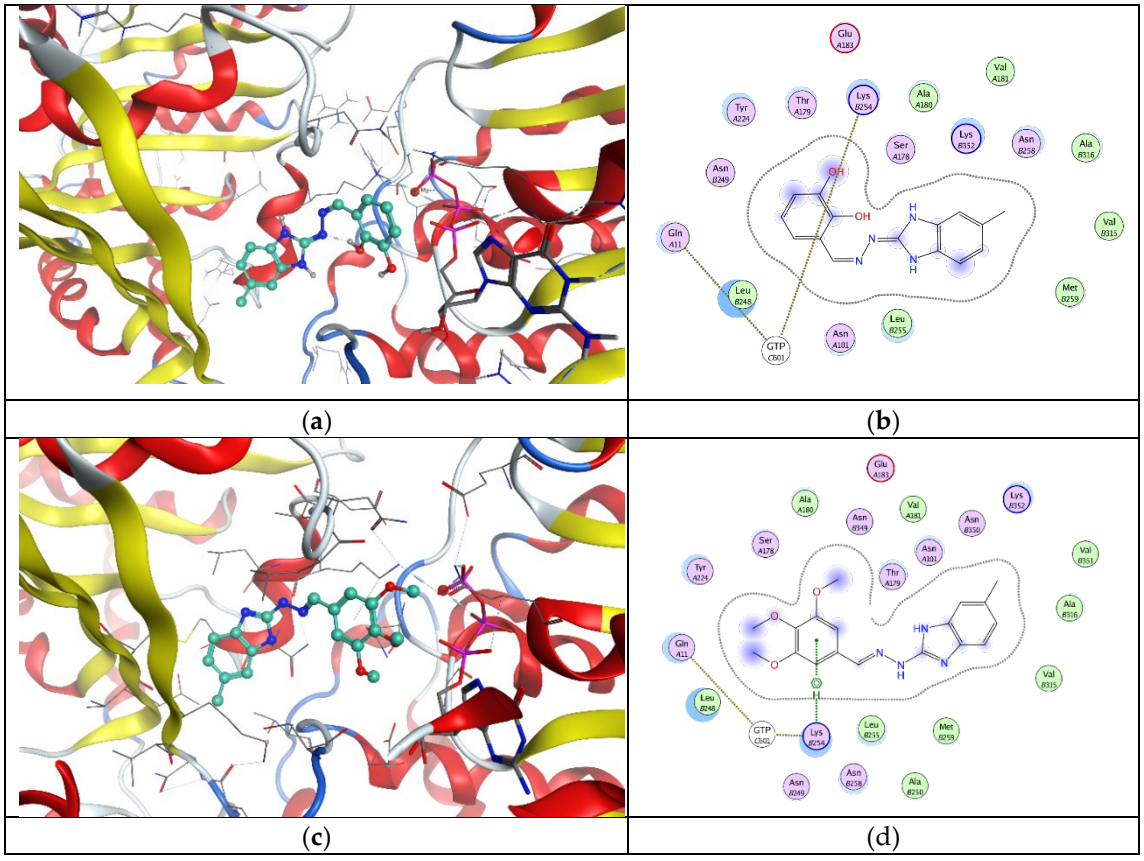

Figure 4. Interactions of ligands **5a-d** at the colchicine binding site of the tubulin dimer: three-dimensional representation of the ligands poses (left part) and interaction maps (right part); the following colors have been used to depict the different components: proximity contour – black dotted line, polar amino acids – pink, lipophilic amino acids – green, basic amino acids – blue, acidic amino acids – red; hydrogen bond interactions – blue arrows, lipophilic interactions – green dotted lines. Docked ligands **5a-d** are shown by balls and sticks; GTP is shown by sticks.

 doi:10.20944/preprints202403.1210.v1

2.3. Determining Cell Viability by MTT Assay

To determine cell viability after treatment with 1H-benzimidazole-2-yl hydrazones **5a-d**, a MTT test was performed and IC_{50} values were calculated as described in Materials and methods. Based on our results, some interesting structure-activity relationships (SAR) could be concluded. As shown in Table 2 the strongest inhibitory effect on cell viability after 48 h of incubation showed substance **5d** followed by **5c** and **5a**. Substance **5b** exhibited the least cytotoxic effect. The antiproliferative effect of all substances is more prominent after 72 hours of treatment. The best cytotoxic results were obtained for the derivatives containing a methyl functional group at the 5(6)-position of the benzimidazole ring. Particularly, a CH_3 group in 5(6)-postion of the benzimidazole heterocycle and a substitution with three methoxy groups at R3, R4 and R5 position of the phenyl ring (forming colchicine-like moiety) proved to be the most potent antiproliferative compound against triple negative breast cancer cell line MDA-MB-231 (Table 2). The next cytotoxic compound also contained a CH_3 group in 5(6)-position of the benzimidazole ring, but two OH substituents in the phenyl ring, forming cathechol-like moiety (Table 2). Indeed, compounds **5a–b** exhibited less cytotoxic activity than compounds **5d–c**, proving the advantage of the presence of a methyl functional group at the 5(6)-position of the benzimidazole ring for anticancer activity. Interestingly, the least cytotoxic compound **5b** against triple negative breast cancer cell line MDA-MB-231 showed the most remarkable cytotoxicity (1.2 ± 0.2) for the hormone-dependent MCF-7 cell line among the previously studied series of 1H-benzimidazole-2-yl hydrazones without substituent in the benzimidazole ring [29]. One explanation may be a less pronounced mitotic arrest in triple-negative breast cancer cells than MCF-7 cells treated with anticancer drugs [34]. However, we proved that an incorporation of the drug in fluorescent micellar carriers improves its cytotoxicity about four times [35].

Table 2. Calculated IC_{50} for each compound 48 and 72 h post incubation with MDA-MB-231.

Compound	IC_{50} (μM)	
	48 h	**72 h**
	Unsubstituted benzimidazole ring	
5a	43.93 ± 9.3	16.04 ± 2.2
5b	60.08 ± 15.3	20.30 ± 4.3 [1]
	5(6)-Methyl benzimidazole ring	
5c	47.28 ± 8.0	14.83 ± 3.8
5d	40.3 ± 4.1	12.65 ± 2.5
	Reference compound	
Nocodazole	0.38 [2]	

[1] [35]; [2] IC_{50} for 24 h [23].

2.4. Investigation of Microtubule Organization and Nuclear Morphology

Immunofluorescence staining was performed from the 6th to the 48th hour to study the effect of the substances on microtubule organization in living cells. While untreated control cells continued to proliferate and had normal cell morphology after 48 h (Figure 5a), exposure to nocodazole (positive control) resulted in visible cell and nuclear shape abnormalities already after 24 h (Figure 5b – white and yellow triangles).

 doi:10.20944/preprints202403.1210.v1

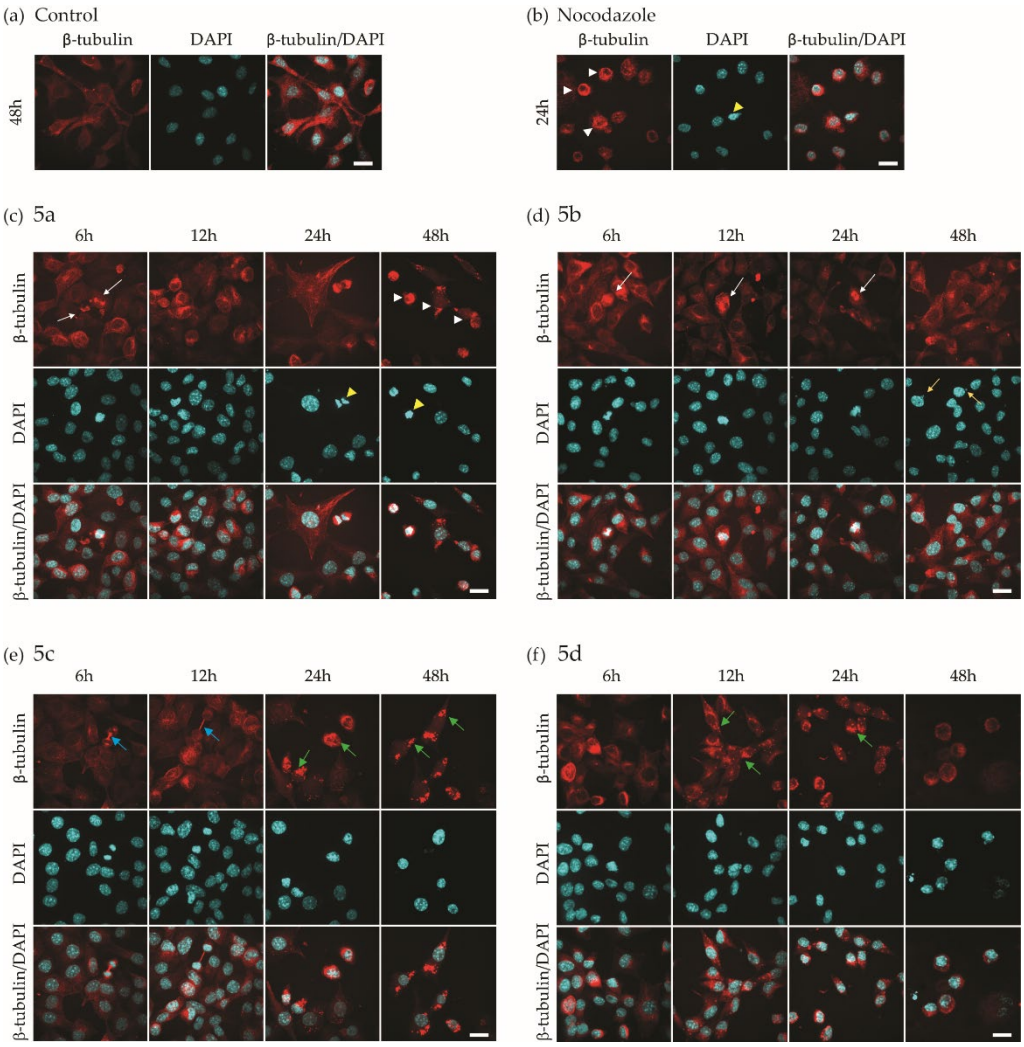

Figure 5. Microtubule organization (β-tubulin) and nuclear morphology (DAPI) of MDA-MB-231. (**a**) negative control – 48 h incubation; (**b**) Nocodazole (positive control) – 24 h treatment; **5a** (**c**), **5b** (**d**), **5c** (**e**) and **5d** (**f**) after treatment with IC_{50} values of the compounds for 6, 12, 24 and 48 h. White arrowheads – abnormal cell morphology; yellow arrowheads – abnormal nuclear morphology; white arrows – mitotic spindle; yellow arrows - micronuclei; green arrows – tubulin aggregates; blue arrows – polar microtubules of the mitotic spindle. Scale bar - 20 μm.

Compound **5a** acts as a strong inhibitor of microtubule dynamics, as no cell division was observed after 6 h of treatment (Figure 5c). Moreover, the cells gradually lost their normal morphology. One of the functions of the microtubules is maintenance of the nuclear structure, which is compromised after 24 h of treatment with **5a** (Figure 5c - yellow triangles). After 48 h, the cells completely lost their normal morphology, although they were still viable (Figure 5c - white triangles).

Compound **5b** caused no inhibition of mitotic spindle formation up to 24 h after treatment (Figure 5d - white arrows). After 48 h of treatment, cells with micronuclei were observed (Figure 5d - yellow arrows). Micronuclei are usually formed as a result of improper formation of the mitotic spindle and the uneven distribution of chromosomes, which leads to their rupture [36]. Therefore, although microtubule polymerization is not completely inhibited, it is visibly affected by compound **5b** after 48 hours. Similar results were obtained for this compound by us earlier in a slightly different period of time [35].

In comparison, cells treated with compound **5c** underwent mitosis within the first 6 hours of treatment since polar microtubules of the mitotic spindle in telophase can be observed (Figure 5e – blue arrows). These structures were still visible and appeared elongated after 12 h, suggesting a

 doi:10.20944/preprints202403.1210.v1

blockage in tubulin depolymerization. Moreover, cytoplasmic tubulin aggregates similar to those seen after treatment with **5d** were also present 24 h post-treatment (Figure 5e – green arrows).

The most cytotoxic compound **5d** caused blockage of mitotic phases in any time frame of the immunofluorescence staining experiment. Cytoplasmic tubulin aggregates were visible 12 h after treatment (Figure 5f – green arrows) which might explain the inability of the cells to undergo mitosis. Following 48 h of incubation, the cell and nuclear morphology were severely altered.

The observed changes in mitosis occurrence, nuclear and cellular shape and tubulin structures after treatment with compounds **5a-d** are summarized in Table 3.

Table 3. Calculated IC_{50} for each compound 48 and 72 h post incubation with MDA-MB-231.

Compound	Characteristics			
	Mitosis	Morphology		Tubulin
		Nucleus	Cell	
Unsubstituted benzimidazole ring				
5a	Until 6 h	Abnormal shape	Abnormal shape	Abnormal mitotic spindle
5b	Until 24 h	Micronuclei	Not affected	Not directly observed
5(6)-Methyl benzimidazole ring				
5c	Until 12 h	Not affected	Not affected	Elongated polar microtubules, cytoplasmic granules
5d	Arrested in mitosis	Abnormal shape	Abnormal shape	Cytoplasmic granules
Reference compound				
Nocodazole	Arrested in mitosis [1]	Abnormal shape	Abnormal shape	Abnormal mitotic spindle

[1] Ref. [5].

These results indicate that compound **5d** is most prominent in disrupting microtubule organization and blocking mitosis in MDA-MB-231 cells. Compound **5a** showed an abnormal mitotic spindle, irregular nuclear and cell shape, and caused delayed mitotic arrest. The abnormalities observed in the microtubules and presence of micronuclei in cells treated with **5c** and **5b** later (after 12/24 h) also led to mitotic arrest.

2.5. Evaluation of antioxidant Activity – Radical Scavenging Properties/Anti-Radical Activity

Two in vitro spectrophotometric systems were used to estimate the effect of the tested derivatives on reactive oxygen species (ROS) concentration. As a first step, the compounds' capability to react with the hypochlorite ions was determined. The second system characterized their potency to scavenge hydrogen peroxide. In both systems, the potency of the compounds is illustrated by the sample/control absorbance ratio in percentage. It demonstrates the capability of 1H-benzimidazole-2-yl hydrazones **5a-d** to scavenge the used in the system ROS. Lower values of the absorbance ratio correspond to better scavenging activity.

The scavenging activity of **5a-d** against the hypochlorite ions is summarized in Figure 6. The effect of the compounds was tested in a concentration range below 50 μM, and all compounds demonstrated scavenging activity. The measured effect was concentration-dependent i.e., the higher the compounds' concentration, the more pronounced the scavenging capability. Compounds **5b** and **5d** denoted modest potency in this system. In the samples containing **5b**, the absorbance ratio has decreased from 98% (11.6 μM) to 85% for the maximal tested concentration of 46.5 μM and for 5d – from 92 % to 81% respectively. On the other side, **5a** at 46.5 μM final concentration of the tested compound in the measurement composition decreased the absorbance ratio to 16%. For **5c** the absorbance ratio decreased to 12%.

 doi:10.20944/preprints202403.1210.v1

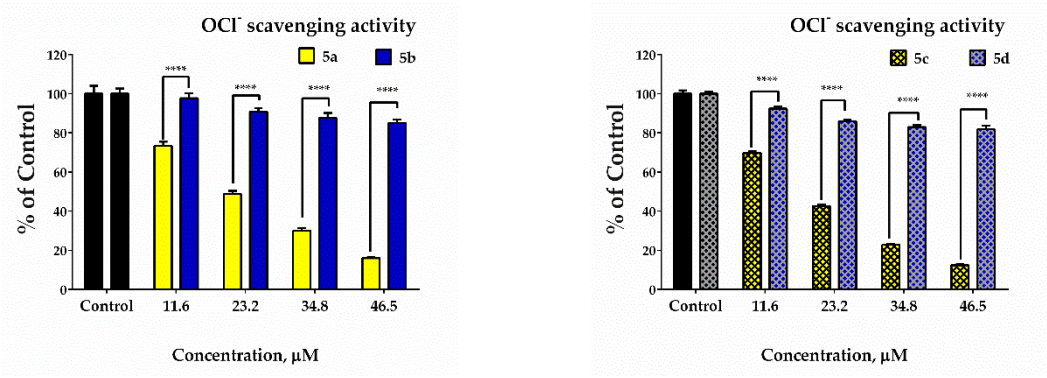

(a) (b)

Figure 6. Scavenging activity of the tested hydrazones: unsubstituted benzimidazole derivatives (**a**) and 5(6)-methylbenzimidazole derivatives (**b**) in a hypochlorite-containing model system. 1 mL reaction mixture contains 15 mM taurine, 0.06 mM NaOCl and the hydrazones in the indicated concentrations. After 5 min incubation, 20 mM KJ was added. Data are presented as means from three independent experiments ± SD. One-way ANOVA, followed by the Bonferroni post-test, was used for statistical evaluation. Differences at $p < 0.05$ were considered statistically significant. * $p < 0.05$, ** $p < 0.01$, *** $p < 0.001$ and **** $p < 0.0001$.

The potency of the studied 1H-benzimidazole-2-yl hydrazones to decrease H_2O_2 concentration is displayed in Figure 7. Due to the lower compounds effect, the concentration range for scavenging capability estimation was increased approximately 10 times. The impact of the compounds was determined at concentrations above 11 μM. In this system, again, most of the compounds demonstrated good linearity of their effectiveness (**5a**: $R^2 = 0.96$; **5b**: $R^2 = 0.96$; **5c**: $R^2 = 0.96$; **5d**: $R^2 = 0.84$). The scavenging activity was concentration-dependent. From the two hydrazone derivatives without substituent in the benzimidazole ring at the maximal tested concentration, **5a** denoted better efficiency and decreased the absorbance ratio by more than 60%. At the other lower tested concentrations, both compounds exhibited similar or very close effects. From the two 5(6)-methylbenzimidazole derivatives, **5c** demonstrated better scavenging activity than **5d** at all concentrations, where both compounds exhibited a statistically significant difference in the tested system properties. Comparing the potency of the compounds unsubstituted in the benzimidazole ring vs. the methyl-substituted ones, both 5(6)-methylbenzimidazole hydrazones had a more pronounced effect compared to the unsubstituted benzimidazole derivatives at the two highest tested concentrations (286 μM and 429 μM).

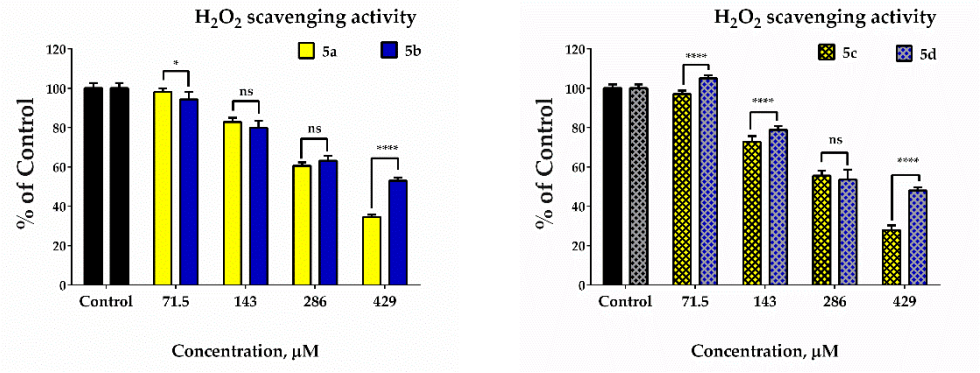

(a) (b)

Figure 7. Scavenging activity of the tested hydrazones: unsubstituted benzimidazole derivatives (**a**) and 5(6)-methylbenzimidazole derivatives (**b**) in hydrogen peroxide-containing model system. 1 mL reaction mixture contained: 0.05 mM $FeCl_2$, 0.2 mM ortho-phenanthroline, 5 mM H_2O_2 and the tested hydrazones. Data are presented as means from three independent experiments ± SD. One-way ANOVA, followed by the Bonferroni post-test, was used to perform the statistical evaluation.

 doi:10.20944/preprints202403.1210.v1

Differences at $p < 0.05$ were considered statistically significant. * $p < 0.05$, ** $p < 0.01$, *** $p < 0.001$ and **** $p < 0.0001$.

To explain the observed effect in the H_2O_2-containing system – whether it is due to a direct scavenging effect or a possible interference with chelation activity, an ortho-phenanthroline chelation test was also performed for verification. The results from the chelation test are presented in Figure 8.

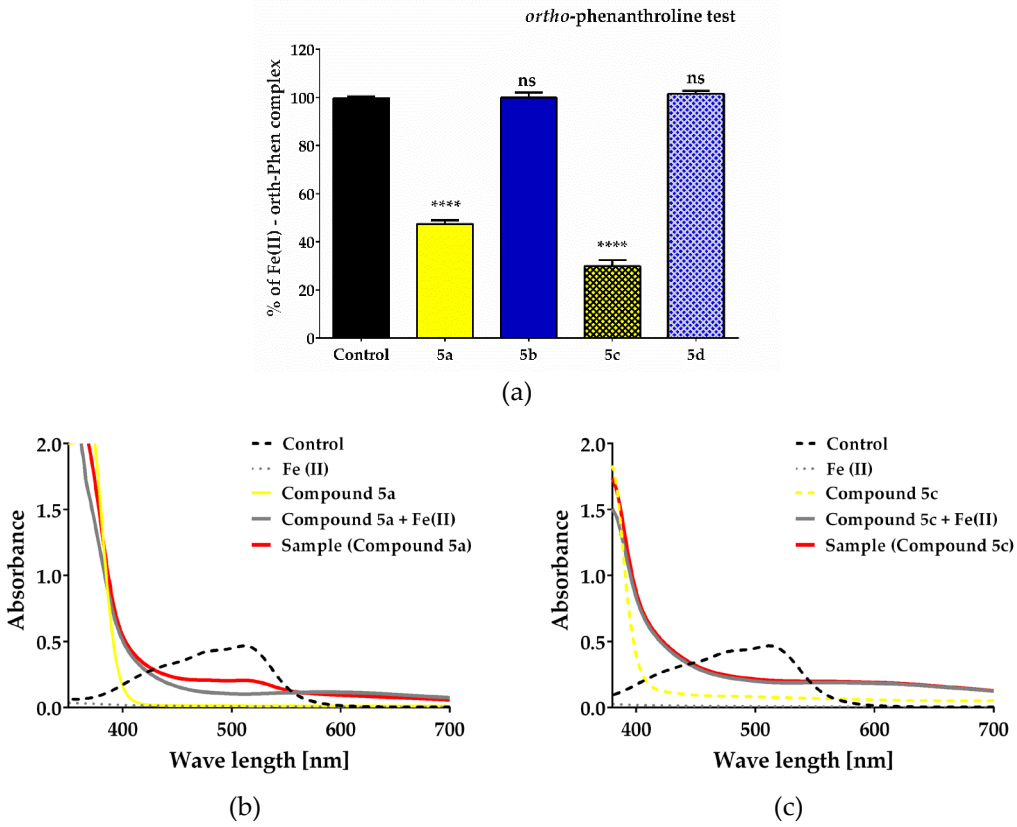

Figure 8. (**a**) Bar diagram showing the extent of formation of the Fe(II)-ortho phenanthroline complex. Data are presented as means from three independent experiments ± SD. One-way ANOVA, followed by the Bonferroni post-test, was used to perform the statistical evaluation. Differences at $p < 0.05$ were considered statistically significant. * $p < 0.05$, ** $p < 0.01$, *** $p < 0.001$ and **** $p < 0.0001$; (**b**) and (**c**) Absorbance spectra of: control - standard orange-red Fe(II)-1,10-phenantroline complex; hydrazone [0.2 mmol/L] alone and in the presence of Fe(II) [0.05 mM]; and the sample solution containing 1,10 phenanthroline [0.2 mM], Fe(II) [0.05 mM] and the hydrazone [0.2 mM].

From the obtained data (Figure 7a), it is evident that there are differences in the amount of generated Fe(II)-ortho-phenanthroline complex in the presence of the tested compounds. In the samples containing **5b** and **5d** the generated amount is the same as in the control sample (99.9 % and 101.6%), suggesting no chelation activity of these hydrazones. In the samples containing **5a** and **5c** the amount of Fe(II)-ortho-phenanthroline complex formation decreased respectively two times (47.5 %) and three times (30.0 %) compared to the control and the trimethoxy compounds. The absorbance spectra of **5a** and **5c**, measured with and without Fe(II), indicate that the presence of iron in the sample mixture is associated with increased absorbance of the solution at a wavelength higher than 400 nm (Figure 8b,c). The absorbance spectra measured in the presence of ortho-phenanthroline, hydrazones **5a** and **5c**, and Fe(II) showed changes compared to the Fe(II)–ortho-phenanthroline complex, suggesting a potency of both compounds to chelate iron. In the sample containing **5a**, some extent of generation of the Fe(II)–ortho-phenanthroline complex has been observed, whereas in the reaction mixture containing **5c**, the absorbance spectra of the sample and the solution containing **5c** and Fe(II) are identical. The latter indicated full suppression of the Fe(II)–ortho-phenanthroline complex

 doi:10.20944/preprints202403.1210.v1

generation in the presence of **5c**. The results from the Fe(II)–ortho-phenanthroline test comply well with the metal-chelating activity of **5a** and **5b** found earlier by HORAC assay [29]

Both investigated ROS have been cited in the literature as having a dual role in cancer development. Hypochlorous acid is released by activated white blood cells during pro-inflammatory states. It is produced during the respiratory burst by neutrophils. During this process, hydrogen peroxide (H_2O_2) is used to induce the oxidation of CI- ions catalyzed by neutrophil-derived myeloperoxidase (MPO) [37]. Conversion of this normally very unreactive halide ion into hypohalous acids means generating strong oxidizing agents capable of exerting aggressive oxidative interactions with the functional groups of various biologically important molecules and causing tissue damage [38,39]. It is thought to be important in the progression of several diseases, including cancer - hypochlorite-induced oxidative stress has been proven to elevate the capability of high-density lipoprotein (HDL), in promoting breast cancer metastasis [40]. Cancer cells produce more H_2O_2 than healthy normal cells [41]. They are known to maintain higher intracellular H_2O_2 concentration and to be capable of tolerating it. H_2O_2 has been reported as taking part in processes like the initiation of DNA alterations, cell proliferation, metastasis, angiogenesis and etc. Data showing evidence that H_2O_2 can sensitize the tumor cells and serve as an anticancer prodrug generating apoptosis have also been published [42].

The extent of the observed effect in the used systems depended on the ROS used in the system and the types of structural modifications of the compounds. In the hypochlorite system, **5a** and **5c** had statistically significant higher scavenging activity in the studied concentration range ($p<0.0001$) compared to both trimethoxy-bearing compounds (**5b** and **5d**) at all tested concentrations and behave as a potent scavenger of hypochlorite ions. All hydrazones denoted the capability to decrease the absorbance signal in the system containing H_2O_2 but have weaker scavenging activity compared to the hypochlorite containing system. This could be attributed to the lower reactivity of H_2O_2 compared to the hypochlorite ion. The principle of the H_2O_2 scavenging assay is based on the formation of the red-orange tri-phenanthroline complex between ferrous ion Fe (II) and 1,10-phenanthroline with maximum absorbance at 515 nm and the capability of H_2O_2 to oxidize all Fe(II) to Fe(III) and prevent complex formation if added before 1,10-phenanthroline to the reaction mixture. In the case of **5b** and **5d** the effect in the H_2O_2-containing system could be attributed only to scavenging activity due to the lack of chelation potential of these compounds. **5a** and **5c** have been proven to possess chelation activity against Fe(II). Given the concentration range that was studied, their H_2O_2 scavenging capability by direct interaction with H_2O_2 is more probable. The data obtained by us are in accordance with our previous investigations of benzimidazoles proving better scavenging activity against stable free radical and antioxidant effect in model systems of iron induced oxidative damage of biologically important molecules in the case of hydroxy-substituted derivatives. This paper demonstrated that this is relevant for other biologically important ROS like H_2O_2 and hypochlorite ion as well. The potency for chelation activity, which is also essential from the point of view of an anti-cancer therapeutic strategy, has also been ascertained for the hydroxy-substituted derivatives.

3. Materials and Methods

3.1. Reagents and Materials

The synthetic chemicals (o-phenylenediamine, 98%, 3,4-diaminotoluene, 97% and the benzaldehydes 2,3-dihydroxybenzaldehyde and 3,4,5-trimethoxybenzaldehyde) were purchased from Sigma Aldrich (Germany) and Alfa-Aesar (United Kingdom).

Thin layer chromatography (TLC) was used for monitoring the reactions and was performed on ALUGRAM SIL G/UV254 pre-coated aluminium sheets with silica gel 60, 0.20 mm thick (Macherey-Nagel, Germany), eluted by benzene-methanol (3:1, v/v) visualized by UV light (λ = 254 nm). The melting points (mp) were determined using Büchi B-540instrument (Büchi Labortechnik AG, Flawil, Switzerland) and were uncorrected. The compounds were characterized by FT-IR spectroscopy and the spectra were obtained on a Bruker Invenio R FT spectrometer in solid state in ATR state on a diamond accessory, 64 scans at 2 cm-1 resolution. ^{1}H and ^{13}C NMR spectra were registered on a

 doi:10.20944/preprints202403.1210.v1

Bruker Avance II+ 600 MHz NMR instrument in solvent DMSO-d_6. Chemical shifts (δ) are reported in parts per million (ppm), coupling constants (J) are given in Hz and splitting patterns were showed as s (singlet), d (doublet), t (triplet) and m (multiplet).

3.2. Synthesis

The methodology for synthesis of 1*H*-benzimidazol-2-yl-thiols **2.1-2.2**, 1*H*-benzimidazol-2-yl-sulfonic acids **3.1-3.2** as well as 1*H*-benzimidazol-2-yl-hydrazides **4.1-4.2** was described in previous publications [27,28].

The general procedure for preparation of 2-[2-benzylidenehydrazinyl]-1*H*-benzimidazole **5a-d** is the following: 2,3-Dihydroxy- or 3,4,5-trimethoxybenzaldehyde (0.002 mol) was added to a mixture of equimolar amount of 5(6)-methyl-1H-benzimidazol-2-yl-hydrazine **4.2** (0.002 mol) in absolute ethanol (5 ml) and the solution was refluxed until the reaction was completed (appr. 3–4 hours). TLC (benzene:methanol = 3:1) was used for monitoring the reaction. The precipitated product was filtered off, washed with ethanol and recrystallized twice from ethanol.

Detailed description of the synthesis of **5a** and **5b** is provided in [28].

2-(2,3-Dihydroxybenzylidene)-1-(5(6)-methyl-1H-benzimidazol-2-yl)hydrazine (**5c**):

Yield: 86%; Mp 285.0-287.1°C; Rf = 0.22 (benzene : methanol = 3:1, v/v); IR (νmax/cm-1): 3378 νN-H), 3058 (νCHarom), 2911 (νasCH$_3$), 2850 (νsCH$_3$), 1649 (δNH), 1614 (νC=N), 1467 (δasCH$_3$), 1381 (δsCH$_3$), 1261 (νAr-O), 715 (γC-H); ^{1}H NMR (600 MHz, DMSO-d_6) δ (ppm): 11.36 (bs, 1H, NH), 9.34 (s, 1H, OH), 8.28 (s, 1H, N=CH), 7.17-7.16 (d, J = 7.47 Hz, 1H, Ar), 7.06-7.04 (d, J = 7.82 Hz, 1H, Ar), 6.99 (s, 1H, Ar-bz), 6.77-6.75 (m, 2H, Ar-bz), 6.69-6.67 (t, J = 7.73, 15.52 Hz, 1H, Ar), 2.32 (s, 3H, CH$_3$-bz); ^{13}C NMR (150 MHz, DMSO-d_6) δ (ppm): 145.89, 121.46, 119.40, 116.09, 21.70.

2-(3,4,5-Trimethoxybenzylidene)-1-(5(6)-methyl-1H-benzimidazol-2-yl)hydrazine (**5d**):

Yield: 75%; Mp 224.6-227°C; Rf = 0.50 (benzene : methanol = 3:1, v/v); IR (νmax/cm-1): 3257 (νN-H), 3012 (νCHarom), 2958 (νasCH$_3$), 2848 (νsCH$_3$), 1648 (δNH), 1612 (νC=N), 1458 (δasCH$_3$), 1381 (δsCH$_3$), 1271, 1047 (νC-O-C), 799 (γC-H); ^{1}H NMR (600 MHz, DMSO-d_6) δ (ppm): 11.38 (bs, 1H, NH), 7.95 (s, 1H, N=CH), 7.17-7.05 (m, 4H, Ar, Ar-bz), 6.82-6.76 (m, 1H, Ar-bz), 3.89-3.70 (d, J = 7.87 Hz, 9H, OCH$_3$), 2.35 (s, 3H, CH$_3$-bz); ^{13}C NMR (150 MHz, DMSO-d_6) δ (ppm): 153.12, 138.22, 130.71, 103.84, 60.08, 56.03, 21.24.

3.3. In Vitro Tubulin Polymerization Assay

The effect of the studied compounds on the polymerization of purified porcine tubulin was evaluated using a commercial assay kit (cat. number BK006P, Cytoskeleton, USA). Fresh buffer solution (PB-GTP) containing polymerization buffer (100 µl volume of 3 mg.ml-1 tubulin in 80 mM piperazine-N,N′-bis(2-ethanesulfonic acid) (PIPES) pH 6.9, 0.5 mM EGTA, 2 mM MgCl, 1 mM GTP, 10% glycerol) was prepared before use. Then, the stock solution of pure bovine tubulin (240 µM) dissolved in the PB-GTP was diluted four-fold to obtain 60 µM tubulin concentration before adding the tested compounds. Stock solutions of the test samples were prepared at a concentration of 700 µM in dimethylsulphoxide (DMSO). Paclitaxel (700 µM) and nocodazole (700 µM) in DMSO were used as positive controls and were provided by the supplier. Before use, the test and control samples were dissolved in PB-GTP to obtain a final concentration of 70 µM. PB-GTP, protein, and sample solutions were kept up to one hour on ice. Keeping the 96-well plate on ice in one well were mixed 60 µL of 60 µM tubulin and 10 µL of 70 µM of the test samples or positive control. To evaluate the spontaneous polymerization of tubulin, in the control experiments to 60 µL of 60 µM tubulin was added 10 µL buffer. Then, the microplate with loaded reaction mixtures was incubated for 90 min at 37°C in the thermostated spectrophotometer chamber. The turbidity of the mixtures was measured at 350 nm every 30 sec. The experiment was performed on SpectroStar Nano (BMG Labtech) equipped with software for kinetic measurements.

 doi:10.20944/preprints202403.1210.v1

3.4. Cell Lines

To determine the cytotoxic potential of the selected substances the human epithelial breast cancer cell line MDA-MB-231 (American Type Culture Collection (ATCC), USA) was used. The cells were cultured in DMEM (Dulbecco's modified essential media) (cat. no. 30-2002, ATCC, Manassas, Virginia, USA) with 10% fetal bovine serum (FBS) (cat. no. F7524, Sigma-Aldrich Co. LLC, St. Louis, MO, USA), 1 mM L-glutamine (cat. no. G7513, Sigma-Aldrich Co. LLC, St. Louis, MO, USA) and penicillin/streptomycin/amphotericin B (100 units/mL: 10 mg/mL: 25 μg/mL) (cat. no. A5955, Sigma-Aldrich Co. LLC, St. Louis, MO, USA) at 37°C, 5% CO2 and optimal humidity.

3.5. Cell Viability Assay

Cells' viability was measured via the (3-(4,5-dimethylthiazol-2-yl)-2,5-diphenyl tetrazolium bromide (MTT, cat. no. 475989, Calbiochem, Merck KGaA, Darmstadt, Germany) assay [43]. Briefly, the cells were trypsinized after reaching 80-90% confluence and seeded in 96-well plates with a concentration of 1×10^4 cells/well, and left to adhere for 24 hours. After the incubation period, the cells were treated with substances **5a**, **5b**, **5c**, and **5d** at concentrations ranging from 1 to 150 μM for 48 and 72 hours. Cells treated with DMSO at a concentration corresponding to the highest concentration in the samples (0.71%), were used as a solvent control. Untreated cells were used as a negative control. After the incubation period, 20 μL of MTT reagent (5 mg/mL) were added to the cells, incubated for 3 h, 37°C, 5% CO_2, which were then dissolved in 5% formic acid in isopropanol. Absorbance was detected at 570 nm on Tecan Infinite F200 PRO plate reader (Tecan GmbH, Salzburg, Austria). The cytotoxicity of the selected compounds was reflected by cell viability as a percentage of the negative control. The half-maximal inhibitory concentration (IC_{50}) was determined using the GraphPad Prism 5 programme (GraphPad Software, San Diego, CA, USA). IC_{50} value of **5b** substance for 72 hours' incubation was estimated earlier [35].

3.6. Immunofluorescence

Immunofluorescence of β-tubulin was performed in order to determine the in vitro effect of the selected compounds on microtubule organization in MDA-MB-231 cell line. Briefly, cells were seeded on cover slides in 24-well plates at a concentration of 5×10^4 cells/well and incubated for 24 hours until complete adhesion. The cells were then treated with the pre-determined 48 h IC_{50} concentrations of compounds **5a**, **5b**, **5c** and **5d**. To monitor the effect of the compounds over time, several incubation time frames of 6, 12, 24 and 48 h were used. A positive control of cells, exposed to 0.38 μM nocodazole (Cat. No. CS210568, Merck Milipore, Massachusetts, USA) [23] for 24 h was also used. After the allotted treatment time, the cells were fixed with 4% paraformaldehyde, permeabilized with 0.5% Triton X-100, blocked with 1% bovine serum albumin (BSA) in phosphate buffer saline, pH 7.4 with 0.1% Tween 20, and labeled with rabbit monoclonal antibody against β-tubulin (1:500, Cat. No. 32-2600, Invitrogen, Waltham, Massachusetts, USA) for 1 hour at room temperature. A donkey anti-rabbit secondary antibody conjugated to TRITC (1:1000, Cat. No. sc-2781, Santa Cruz Biotechnology, USA) was attached to the primary antibody. Finally, cell nuclei were stained for 5 min at room temperature in dark with 1 μg/mL 4',6-diamidino-2-phenylindole (DAPI, D9542, Sigma-Aldrich Co. LLC, St. Louis, MO, USA). Fluorescence microscopy was performed on a spinning disk confocal microscope (Andor Revolution XD) at 63x magnification. The obtained data were analyzed with Fiji [44].

3.7. Hypochlorite Scavenging Activity

The assay was performed according to Weiss et al. [45]. 1 mL reaction mixture contains 50 mM PB (K_2HPO_4/KH_2PO_4 buffer, pH 7.4), 15 mM taurine, 0.06 mM NaOCl and the tested compounds. In controls, no hydrazones were added. After incubation for 5 min at 37°C, 20 mM KJ was added. The solutions of taurine and KJ were prepared just before being used in distilled water. Sample absorbance was measured at 350 nm using spectrophotometer GENESYS 50 UV-VIS .

 doi:10.20944/preprints202403.1210.v1

3.8. Hydrogen Peroxide Scavenging Activity

The experiment was performed according to Mukhopadhyay et al. [46]. The reaction mixtures were with a final volume of 1 mL and contained the following reagents: 0.05 mM $FeCl_2$, 0.2 mM ortho-phenanthroline, 5 mM H_2O_2 and the tested hydrazones. A 5 min incubation followed the addition of the H_2O_2 to the mixture containing the investigated compounds and Fe (II). After a second incubation of 10 min, ortho-phenanthroline was added. The samples' absorbances were measured at 515 nm at spectrophotometer GENESYS 50 UV-VIS . The control sample showed maximum absorbance. It contains only ferrous irons and ortho–phenanthroline.

3.9. Ortho-Phenanthroline Test

We used the ortho-phenanthroline method to examine the hydrazones' iron-chelating properties. 1 mL sample solution of 50 mM PB, pH 7.4, contains 0.2 mM ortho-phenanthroline and 0.05 mM $FeCl_2$, and 0.2 mM tested hydrazones. In controls, the tested compounds were omitted. As the first step, mixtures containing the ferrous iron and the hydrazones were prepared. They were allowed to react for 5 min – the time necessary for the formation of complexes between Fe(II) and the tested compounds if chelation properties are being observed. The second step comprises the addition of the ortho-phenanthroline solution. Absorbance was measured at 515 nm via GENESYS 50 UV-VIS in order to determine the colored complexes formation between ortho-phenanthroline and the remaining free ferrous irons [47]. The results have been presented as a percentage of the control sample. Absorbance spectra of all the samples, the controls and the measurement compositions containing the tested hydrazones and Fe(II) at the concentrations used in the samples have been taken.

3.10. Molecular Docking

Docking was performed by the Molecular Operating Environment (MOE) 2020 software package [30]. The model was built upon the structure of $\alpha\beta$-tubulin with the stathmin-like domain of the RB3 protein in complex with colchicine and vinblastine, obtained by XRD with an overall resolution of 4.10 Å resolution, PDB ID: 1Z2B [31]. The structure was protonated (pH 7.0, 300K, Salt 0.1M/L) using the 3D protonation algorithm implemented in the MOE package. Different conformations of the studied compounds were included in the docking study accounting for amino and imino tautomeric forms, E and Z configuration of the azomethyne double bond, s-cis and s-trans arrangement of the substituents around the N-N bond, formation of intramolecular hydrogen bonds etc. All conformations of all ligands were docked in the colchicine pocket using the Triangle Matcher algorithm for the initial placement of the structures, which returns up to 10E6 poses of the ligand inside a pocket. These poses were scored by the London dG [30] function which estimates the free energy of the binding of the ligand from a given pose and consists of terms that estimate average gain/loss of rotational and translational entropy and loss of flexibility of the ligand. It measures the geometric imperfections of the hydrogen bonds and the desolvation energy of atoms. The best 50 poses for every ligand were further optimized with the Induced Fit methodology, using the MMFF94x force field/Born solvation model and optimization cutoff of 6Å from the ligand. The GBVI/WSA dG [30] was used as rescoring function and the best 30 poses were collected for further analysis.

5. Conclusions

In this work, a series of benzimidazole derivatives were evaluated for their in vitro anticancer potential against triple negative breast cancer cell line MDA-MB-231. In MTT assay, compound **5d** followed by **5c** displayed significant growth inhibitory activities against cancer cell line MDA-MB-231 comparable to the positive control Nocodazole. The data highlight the role of methyl functional group at the 5(6)-position of the benzimidazole ring of derivatives as suggested the molecular docking studies. The most cytotoxic compound **5d**, combining a methyl group in the benzimidazole ring and colchicine-like fragment in the hydrazone chain, caused tubulin aggregation and blockage

 doi:10.20944/preprints202403.1210.v1

of mitosis in early time of treatment. Following 48 h of incubation, cell morphology and nuclear integrity were destroyed and only cell remnants were present. In the in vitro tubulin polymerization assay **5d** slowed down most significantly the initial rate of tubulin polymerization among the tested compounds – with 4 times reduction compared to the initial rate exhibited by nocodazole. The molecular docking study showed that the binding of the ligands to the colchicine site of tubulin is based mainly on Van der Waals interactions and in the case of **5d** – lipophilic interactions of the trimethoxyphenyl ring with Lys254 from the β-tubulin unit are also involved. The evaluation of the radical scavenging properties and anti-radical activity demonstrated that the promising antiproliferative and related impairment of cancer cell's tubulin dynamics of the compounds is complemented by ability to scavenge biologically important ROS like H_2O_2 and hypochlorite ion as well as chelate metal atoms such as iron.

Supplementary Materials: The following supporting information can be downloaded at: www.mdpi.com/xxx/s1, Figure **S1-S6**. IR and NMR spectra of compounds **5c** and **5d**.

Author Contributions: Conceptualization, D.Y., M.G. and R.Tz.; methodology, D.Y., M.G., N.H., M.R., and R.Tz.; software, N.T..; validation, D.Y., M.R. and R.Tz.; investigation, M.A., I.G., V.M., M.G., N.H., N.T., M.R.; data curation, D.Y., R.Tz.; writing— D.Y., M.A., I.G., V.M., M.G., N.H., N.T., M.R., and R.Tz.; visualization, D.Y., M.A., I.G., V.M., M.G., N.H., N.T., M.R., and R.Tz.; supervision, D.Y., R.Tz.; project administration, D.Y.; funding acquisition, D.Y. All authors have read and agreed to the published version of the manuscript.

Funding: This research was funded by NATIONAL SCIENCE FUND OF BULGARIA, Contract number KP-06-H39/4.

Institutional Review Board Statement: Not applicable

Informed Consent Statement: Not applicable.

Data Availability Statement: Data are available within the article.

Acknowledgments: The authors would like to thank the Bulgarian Advanced Light Microscopy Node of the Euro-BioImaging consortium at the Institute of Molecular Biology, Bulgarian Academy of Sciences for the provided support for the microscopy imaging. Equipment of INFRAMAT (Research Infrastructure from National roadmap of Bulgaria), supported by the Bulgarian Ministry of Education and Science, is used in a part of the present investigations.

Conflicts of Interest: The authors declare no conflict of interest. The funders had no role in the design of the study; in the collection, analyses, or interpretation of data; in the writing of the manuscript; or in the decision to publish the results.

References

1. McKean, P.G.; Vaughan, S.; Gull,K. The extended tubulin superfamily. *J Cell Sci*. **2001**, *114*, 2723–2733.
2. Meiring, J. C. M.; Shneyer,B. I.; Akhmanova,A. Generation and regulation of microtubule network asymmetry to drive cell polarity. *Curr. Opin. Cell Biol*., **2020**, *62*, 86–95.
3. Pellegrini, F.; Budman, D.R. Review: tubulin function, action of antitubulin drugs, and new drug development. *Cancer Invest*. **2005**, *23*, 264-2735.
4. Barlan, K.; Gelfand, V. I. Microtubule-Based Transport and the Distribution, Tethering, and Organization of Organelles. *Cold Spring Harb. Perspect. Biol*. **2017**, *9*, 025817.
5. Kline-Smith S. L.; Walczak, C. E. Mitotic Spindle Assembly and Chromosome Segregation: Refocusing on Microtubule Dynamics. *Mol. Cell* **2004**, *15*, 317–327.
6. Schaefer, K.L.; PPARgamma Inhibitors as Novel Tubulin-Targeting Agents. *PPAR Res*. **2008**, *2008*, 785405.
7. Mukhtar, E.; Adhami, V.M.; Mukhtar, H. Targeting microtubules by natural agents for cancer therapy. *Mol Cancer Ther*. **2014**, *13*, 275-84.
8. Avendaño,C.; Carlos Menéndez, J. Anticancer Drugs Targeting Tubulin and Microtubules. In *Medicinal Chemistry of Anticancer Drugs*, 2nd ed.; Avendaño,C.; Carlos Menéndez, J., Eds; Elsevier, 2015, pp 359-390.
9. Rowinsky, E.; Donehower, R. Antimicrotubule agents. In *DeVita VT*, 5th ed, Hellmann, S.; Rosenberg, S.A., Eds.; Lippincott-Raven: Philadelphia, 1997.
10. Martin,R. J.; Robertson, A.P.; Bjorn, H. Target sites of anthelmintics. *Parasitology* **1997**, *114*, 111-124.
11. Kingston, D. G. I. In *Anticancer Agents from Natural Products*; 2nd ed.; Cragg, G. M.; Kingston, D. G. I.; Newman, D. J. Eds.; CRC Press: Boca Raton, FL, 2005.

12. Steinmetz, M. O.; Prota, A. E. Microtubule-Targeting Agents: Strategies to Hijack the Cytoskeleton. *Trends in Cell Biology* **2018**, *28*, 776-792.
13. Lu, Y.; Chen, J.; Xiao, M.; Li, W.; Miller, D.D. An overview of tubulin inhibitors that interact with the colchicine binding site. *Pharm Res*. **2012**,*29*, 2943-71
14. Van Den Bossche, H.; Rochette, F.; Hörig, C. In Advances in Pharmacology and Chemotherapy; *Academic Press: New York*, **1982**; *19*.
15. Bukhari, S.N.A.; Kumar, G.B.; Revankar, H.M.; Qin, H.-L. Development of combretastatins as potent tubulin polymerization inhibitors. *Bioorg. Chem*. **2017**, 72, 130-147.
16. Uckun, F. M.; Cogle, C. R.; Lin, T. L.; Qazi, S.; Trieu, V. N.; Schiller, G.; Watts, J. M. A Phase 1B Clinical Study of Combretastatin A1 Diphosphate (OXi4503) and Cytarabine (ARA-C) in Combination (OXA) for Patients with Relapsed or Refractory Acute Myeloid Leukemia. *Cancers* **2020**, *12*, 74.
17. Grisham, R.; Ky, B.; Tewari, K.S.; Chaplin, D.J.; Walker, J. Clinical trial experience with CA4P anticancer therapy: focus on efficacy, cardiovascular adverse events, and hypertension management. *Gynecol Oncol Res Pract*. **2018,** *5,* 1.
18. Blay, J.Y.; Pápai, Z.; Tolcher, A.W.; Italiano, A.; Cupissol, D.; López-Pousa, A.; Chawla, S.P.; Bompas, E.; Babovic, N.; Penel, N.; Isambert, N.; Staddon, A.P.; Saâda-Bouzid, E.; Santoro, A.; Franke, F.A.; Cohen, P.; Le-Guennec, S.; Demetri, G.D. Ombrabulin plus cisplatin versus placebo plus cisplatin in patients with advanced soft-tissue sarcomas after failure of anthracycline and ifosfamide chemotherapy: a randomised, double-blind, placebo-controlled, phase 3 trial. *Lancet Oncol*. **2015,** 16, 531-40.
19. Rashid, M.; Husain, A.; Siddiqui, A. A.; Mishra, R. Benzimidazole clubbed with triazolo-thiadiazoles and triazolo-thiadiazines: New anticancer agents. *Eur. J. Med. Chem*. **2013**, *62*, 785-798.
20. Tahlan, S.; Kumar, S.; Kakkar, S.; Narasimhan, B. Benzimidazole scaffolds as promising antiproliferative agents: a review. *BMC Chem*. **2019**, 15, 66.
21. Kamal, A.; Reddy, T. S.; Vishnuvardhan, M.V.P.S.; Nimbarte, V. D.; Subba Rao, A.V.; Srinivasulu, V.; Shankaraiah, N. Synthesis of 2-aryl-1,2,4-oxadiazolo-benzimidazoles: Tubulin polymerization inhibitors and apoptosis inducing agents, *Bioorganic & Medicinal Chemistry* **2015**, *23*, 4608-4623.
22. Miao, T.T.; Tao, X.B.; Li, D.D.; Chen, H.; Jin, X.Y.; Geng, Y.; Wang, S.F.; Gu, W. Synthesis and biological evaluation of 2-aryl-benzimidazole derivatives of dehydroabietic acid as novel tubulin polymerization inhibitors. *RSC Adv*. **2018**, *8*, 17511–17526.
23. Ricart, A.D.; Ashton, E.A.; Cooney, M.M. A phase I study of MN-029 (denibulin), a novel vascular-disrupting agent, in patients with advanced solid tumors. *Cancer Chemother Pharmacol* **2011**, *68*, 959–970.
24. de la Roche, N.M.; Mühlethaler, T.; Di Martino, R.M.C; Ortega, J.A.; Gioia, D.; Royd, B.; Prota, A.E.; Steinmetz, M.O.; Cavalli, A. Novel fragment-derived colchicine-site binders as microtubule-destabilizing agents. *Eur. J. Med. Chem*. **2022**, *241*, 114614.
25. González, L. C.; Espinosa-Mendoza, J. D.; Matadamas-Martínez, F.; Romero-Velásquez, A.; Flores-Ramos, M.; Colorado-Pablo, L. F.; Cerbón-Cervantes, M. A.; Castillo, R.; González-Sánchez, I.; Yépez-Mulia, L.; Hernández-Campos, A.; Aguayo-Ortiz R. Structure-Based Optimization of Carbendazim-Derived Tubulin Polymerization Inhibitors through Alchemical Free Energy Calculations. *J. Chem. Inf. Model*. **2023**, *63*, 7228–7238.
26. Anichina, K.; Argirova, M.; Tzoneva, R.; Uzunova, V.; Mavrova, A.; Vuchev, D.; Popova-Daskalova, G.; Fratev, F.; Guncheva, M.; Yancheva, D. 1H-benzimidazole-2-yl hydrazones as tubulin-targeting agents: Synthesis, structural characterization, an-thelmintic activity and antiproliferative activity against MCF-7 breast carcinoma cells and molecular docking studies. *Chem. Biol. Interact*. **2021**, *345*, 109540.
27. Argirova, M.A.; Georgieva, M.K.; Hristova-Avakumova, N.G.; Vuchev, D.I.; Popova-Daskalova, G.V.; Anichina, K.K.; Yancheva, D.Y. New 1H-benzimidazole-2-yl hydrazones with combined antiparasitic and antioxidant activity. *RSC Adv*. **2021**, *11*, 39848–39868.
28. Argirova, M.; Guncheva, M.; Momekov, G.; Cherneva, E.; Mihaylova, R.; Rangelov, M.; Todorova, N.; Denev, P.; Anichina, K.; Mavrova, A.; Yancheva, D. Modulation Effect on Tubulin Polymerization, Cytotoxicity and Antioxidant Activity of 1H-Benzimidazole-2-Yl Hydrazones. *Molecules* **2023**, *28*, 291.
29. Molecular operating environment (MOE) 2020 Chemical Computing Group Inc., 1010 Sherbooke St. West, Suite #910, Mon-treal, QC, Canada, H3A 2R7.
30. Gigant, B.; Wang, C.; Ravelli, R.B.G.; Roussi, F.; Steinmetz, M.O.; Curmi, P.A.; Sobel, A.; Knossow, M. Structural basis for the regulation of tubulin by vinblastine. *Nature* **2005**, *435*, 519–522.
31. Knossow, M.; Campanacci, V.; Khodja, L. A.; Gigant, B. The Mechanism of Tubulin Assembly into Microtubules: Insights from Structural Studies, *iScience*, **2020**, *23*, 101511.
32. Wang, Y.; Zhang, H.; Gigant, B.; Yu, Y.; Wu, Y.; Chen, X.; Lai, Q.; Yang, Zh.; Chen, Q.; Yang, J. Structures of a diverse set of colchicine binding site inhibitors in complex with tubulin provide a rationale for drug discovery, *FEBS Journal*. **2016**, *283*, 102–111.
33. Blajeski, A.L.; Phan, V.A.; Kottke, T.J.; Kaufmann, S.H. G(1) and G(2) cell-cycle arrest following microtubule depolymerization in human breast cancer cells. *J Clin Invest*. **2002**, *110*,91-9.

 doi:10.20944/preprints202403.1210.v1

34. Bryaskova, R.; Georgiev, N.; Philipova, N.; Bakov, V.; Anichina, K. Argirova, M.; Apostolova, S.; Georgieva, I.; Tzoneva, R. Novel Fluorescent Benzimidazole- Hydrazone-Loaded Micellar Carriers for Controlled Release: Impact on Cell Toxicity, Nuclear and Microtubule Alterations in Breast Cancer Cells. *Pharmaceutics* **2023**, *15*, 1753.
35. Haar, E. T.; Day, B. W.; Rosenkranz, H. S. Direct tubulin polymerization perturbation contributes significantly to the induction of micronuclei in vivo. *Mutat. Res. Mol. Mech. Mutagen*. **1996**, *350*, 331–337.
36. Davies M. J.; Hawkins, C. L. The Role of Myeloperoxidase in Biomolecule Modification, Chronic Inflammation, and Disease. *Antiox. Redox Signal*. **2020,** *32*, 957-981.
37. Davies, M.J. Myeloperoxidase-derived oxidation: Mechanisms of biological damage and its prevention. *J. Clin. Biochem. Nutr*. **2010**, *48*, 8–19;
38. Ramos, D.R.; García, M.V. Canle, M.; Santaballa, J.A.; Furtmüller, P.G.; Obinger, C. Myeloperoxidase-catalyzed chlorination: The quest for the active species. *J. Inorg. Biochem*. **2008**, *102*, 1300–1311.
39. Pan, B.; Ren, H.; Lv. X.; Zhao. Y.; Yu, B.; He, Y.; Ma, Y.; Niu, C.; Kong, J.; Yu, F.; Sun, W.B.; Zhang, Y.; Willard, B.; Zheng, L. Hypochlorite-induced oxidative stress elevates the capability of HDL in promoting breast cancer metastasis. *J. Transl. Med*. **2012**, *30*, 65.
40. Doskey, C.M.; Buranasudja, V.; Wagner, B.A.; Wilkes, J.G.; Du, J.; Cullen, J.J.; Buettner, G.R. Tumor cells have decreased ability to metabolize H_2O_2: Implications for pharmacological ascorbate in cancer therapy. *Redox. Biol*. **2016**, *10*, 274-284.
41. López-Lázaro, M. Dual role of hydrogen peroxide in cancer: possible relevance to cancer chemoprevention and therapy. *Cancer Lett*. **2007**, *252*,1-8
42. Mosmann, T. Rapid colorimetric assay for cellular growth and survival: Application to proliferation and cytotoxicity assays. *J. Immunol. Methods* **1983**, *65*, 55–63.
43. Schindelin, J.; Arganda-Carreras, I.; Frise, E. et al. Fiji: an open-source platform for biological-image analysis. *Nat. Methods* **2012**, *9*, 676–682.
44. Weiss, S. J.; Klein, R.; Slivka, A.; Wei, M. Chlorination of taurine by human neutrophils. Evidence for hypochlorous acid generation. *J. Clin. Invest.* **1982**, *70*, 598-607.
45. Mukhopadhyay, D.; Dasgupta, P.; Sinha Roy, D.; Palchoudhuri, S.; Chatterjee, I.; Ali, S.; Dastidar, S. G. A Sensitive In vitro Spectrophotometric Hydrogen Peroxide Scavenging Assay using 1,10-Phenanthroline. *Free Radicals and Antioxidants* **2016**, *6*, 124-132.
46. Marczenko, Z.; Balcerzak, M. In *Separation, preconcentration, and spectrophotometry in inorganic analysis*. 1st ed.; Kloczko, E., Eds.; Elsevier, 2000, 10, pp 3–521.